



# Thermoresponsive nanocomposites incorporating microplasma synthesized magnetic nanoparticles—Synthesis and potential applications

Hugo Nolan<sup>1</sup>  | Daye Sun<sup>1</sup> | Brian G. Falzon<sup>1</sup> | Paul Maguire<sup>2</sup> |  
Davide Mariotti<sup>2</sup>  | Li Zhang<sup>3</sup> | Dan Sun<sup>1</sup> 

<sup>1</sup> Advanced Composite Research Group ACRG, School of Mechanical, Aerospace Engineering, Queen's University Belfast, Belfast BT9 5AH, UK

<sup>2</sup> Nanotechnology and Integrated BioEngineering Centre (NIBEC), Ulster University, Shore Road, Newtownabbey BT37 0QB, UK

<sup>3</sup> Research Center for Nano-Biomaterials, Analytical & Testing Center, Sichuan University, Chengdu, China

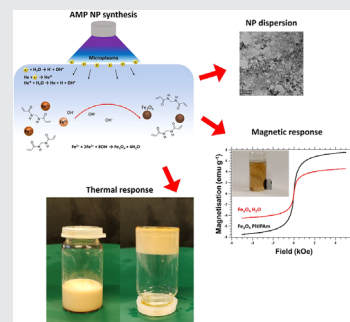
## Correspondence

Dan Sun, Advanced Composite Research Group ACRG, School of Mechanical, Aerospace Engineering, Queen's University Belfast, Belfast BT9 5AH, UK.  
Email: d.sun@qub.ac.uk

## Funding information

Engineering and Physical Sciences Research Council, Grant numbers: EP/P00394X/1, EP/M024938/1

The requirement for novel therapeutic and diagnostic techniques for biomedical applications has driven the development of multifunctional composite materials. This, in turn, has necessitated the use of novel synthesis and processing techniques for scalable nanocomposite production with tuneable material properties. Atmospheric Pressure Microplasma (APM) is a synthesis technique which has received considerable interest in recent years as a viable route for fabrication of nanoparticles (NPs) and NP/polymer composites. Here, we employ APM synthesis of NPs in solutions demonstrating, for the first time, the in situ synthesis of magnetic NPs ( $\text{Fe}_3\text{O}_4$ ) in a hydrogel; fabricating a magnetic thermo-responsive hydrogel (poly (N-isopropylacrylamide)) composite. This demonstrates the applicability of our APM process for producing materials which are potentially relevant to the health sector.



## KEYWORDS

atmospheric pressure plasma, magnetic hydrogel, magnetic nanoparticles, thermo-responsive hydrogel

## 1 | INTRODUCTION

Recent years have seen increased research into the use of non-equilibrium Atmospheric Pressure Microplasma (APM) technology in a wide range of applications.<sup>[1,2]</sup> In particular, the interaction between APM and liquids offers a robust technique for solution processing of nanomaterials due to the enriched chemical environment in the vicinity of the plasma/liquid interface.<sup>[1,3]</sup>

The versatility of APM processing has been demonstrated by the wide variety of nanomaterials synthesized successfully.<sup>[4–6]</sup> In addition to metal NPs, APM processing has also been used in the synthesis and functionalization of other nanostructures such as Si nanocrystals,<sup>[7]</sup> nanocarbon materials,<sup>[8,9]</sup> and metal oxides such as  $\text{Fe}_3\text{O}_4$ ,<sup>[10]</sup>  $\text{Cu}_2\text{O}$ ,<sup>[11,12]</sup> and  $\text{Co}_3\text{O}_4$ <sup>[13]</sup> in aqueous solutions. Therefore, APM techniques have been demonstrated as viable routes to engineering and tailoring the surface/interfacial properties of

This is an open access article under the terms of the Creative Commons Attribution License, which permits use, distribution and reproduction in any medium, provided the original work is properly cited.

© 2018 The Authors. *Plasma Processes and Polymers* Published by WILEY-VCH Verlag GmbH & Co. KGaA, Weinheim

nanomaterials and nanocomposites.<sup>[2,14]</sup> It is suggested that NP synthesis proceeds by different reaction mechanisms, depending on the precursors and solution used. Thus, the variety of possible reaction mechanisms must be taken into consideration when applying APM synthesis techniques to different materials. While much research has explored APM synthesis and processing of various nanomaterials in water, the incorporation of such nanomaterials into a polymeric matrix to form functional nanocomposites, has received limited attention.

Using APM-liquid interactions, we have been able to create complex composites consisting of polymer (e.g., PEDOT:PSS,<sup>[15]</sup> PVA)<sup>[16]</sup> and metal or inorganic materials (e.g., TiO<sub>2</sub>,<sup>[17]</sup> Si nanocrystals,<sup>[18]</sup> metal NPs,<sup>[18]</sup> or boron nitride<sup>[19]</sup>), resulting in improved electrical and thermal performance or promising biomedical applications. The incorporation of NPs in polymer through APM-assisted approaches resulted in improved particle dispersion and stability, highlighting the great potential of APM as a technique for fabrication of advanced functional nanocomposites.

One area of interest in the biomedical field is the development of multifunctional hydrogel-based nanocomposites. Hydrogels are a category of polymers which are highly crosslinked hydrophilic polymer networks consisting of >90% water by mass. Many hydrogels have excellent biocompatibility and exhibit a response to environmental stimuli, such as temperature and/or pH.<sup>[20]</sup> Temperature responsive hydrogels exhibit a phase change from coil to globule polymer structure at the so-called Lower Critical Transition Temperature (LCST). These promising characteristics have encouraged their wide use in applications such as drug delivery, cancer therapy, and tissue engineering.<sup>[21–23]</sup> Further functionality can be introduced by integrating functional NPs with hydrogels to form a nanocomposite, and such systems have shown interesting properties for applications such as anti-microbial, sensing, imaging, drug delivery, cancer therapeutics, and many others.<sup>[24–27]</sup>

Magnetic hydrogels, consisting of magnetic NPs (MNP) incorporated in a hydrogel matrix, exhibit a response to external magnetic field and are of particular value in the biomedical field, including magnetic resonance imaging, drug delivery, and hyperthermia cancer therapy, etc.<sup>[28–32]</sup> While MNPs can be formed from a variety of metals and metal oxides, cobalt or nickel based MNPs are less desirable due to their potential toxicity if no appropriate coatings are employed.<sup>[33]</sup> Iron oxide MNPs are of particular interest as a result of their biocompatibility as well as excellent magnetic response.<sup>[33,34]</sup> Iron oxide based magnetic NPs exist in various forms, with  $\alpha$ -Fe<sub>2</sub>O<sub>3</sub>,  $\gamma$ -Fe<sub>2</sub>O<sub>3</sub>, and Fe<sub>3</sub>O<sub>4</sub> being of particular interest owing to their room temperature superparamagnetic behavior in NPs of diameter less than 15 nm.<sup>[10,33,35]</sup>

Iron oxide based magnetic hydrogels are typically prepared by physically mixing pre-synthesized MNPs with hydrogels.<sup>[36]</sup> These MNPs are mostly synthesized by conventional methods such as co-precipitation,<sup>[37]</sup> thermal decomposition, hydrothermal, or micro-emulsion.<sup>[38]</sup> These techniques suffer from issues such as poor control of MNP size distribution or require elevated temperatures/long processing times. Although the use of stabilizing agents or high-pressure reaction vessels can better control the MNP characteristics, this comes at the cost of significant experimental restrictions. Recent studies reported in situ iron oxide MNP synthesis in the hydrogel matrix based on a co-precipitation method,<sup>[39]</sup> with further effort introducing covalent bonds between pre-formed MNPs and the hydrogel network.<sup>[40]</sup> However the use of potentially hazardous chemicals may create a concern over their use in biomedical applications.

APM synthesis of iron oxide MNPs was recently demonstrated in aqueous solutions.<sup>[10,41]</sup> However, incorporation of APM-synthesized MNPs into a hydrogel and the potential application of such complicated material system has not yet been explored. Herein, we report, for the first time, the in situ APM synthesis of iron oxide MNPs, for the fabrication of a magnetic thermo-responsive (poly (N-isopropylacrylamide), PNIPAm) hydrogel. The properties of resulting hydrogel system have been characterized and the potential application of the materials have been discussed.

## 2 | EXPERIMENTAL

### 2.1 | Materials and methods

Iron (III) chloride (FeCl<sub>3</sub>), iron (II) chloride (FeCl<sub>2</sub>), sodium hydroxide (NaOH), ammonium persulfate (APS), poly-(N-isopropyl acrylamide) (PNIPAm), methylene bisacrylamide (MBAm) and N,N,N',N'-tetramethyl ethylenediamine (TEMED) were purchased from Sigma–Aldrich. All solutions were made using 18.2 M $\Omega$  Millipore water. Argon and helium gases were purchased from BOC.

### 2.2 | Nanoparticle synthesis

FeCl<sub>3</sub> (5 mM) and FeCl<sub>2</sub> (2.5 mM) were dissolved in water which had been thoroughly degassed by bubbling with Ar for at least 30 min. The solution pH was measured using a digital pH meter and was adjusted to pH 5 by adding appropriate amount of NaOH solution (2 M). MBAm (0.5 wt %) was then dissolved in the solution, under Ar protection throughout.

The above solution was then transferred to a bespoke reaction vessel as illustrated in Figure 1. A stainless-steel capillary (inner diameter 250  $\mu$ m, passing helium gas at 50 sccm) acting as the cathode was placed in chamber A,

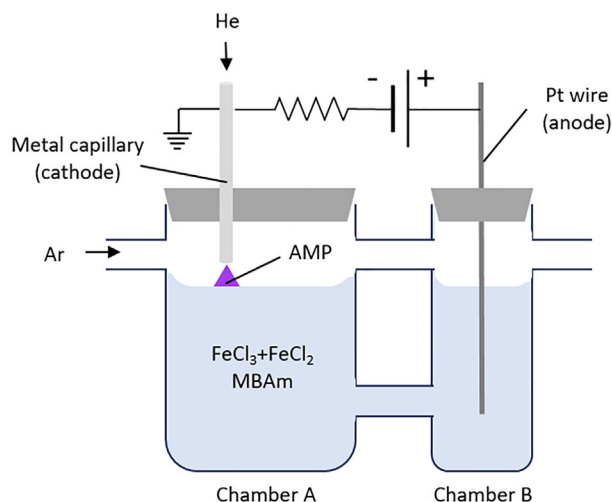


**FIGURE 1** Schematic of the apparatus used for APM synthesis of MNPs in MBAm solution

1.5 mm above the solution surface, and a Pt wire immersing in the solution in the chamber B was used as the anode. Both chambers were under the ambient atmosphere and a flow of Ar was maintained across the vessel headspace at approx. 5 sLm to establish an oxygen-free environment. A steady APM was ignited at the liquid/gas interface and a steady current of 5 mA maintained under a voltage range of 0.7–1 kV. The reaction was allowed to proceed for 30 min under mechanical stirring at approx. 650 rpm. This stirring rate was sufficient to ensure thorough mixing of the solution, but not so fast as to cause significant disturbance to the solution surface. As such, the distance between the capillary tip and liquid surface (length of the AMP jet) was held constant. The solution temperature in chamber A was monitored with a thermocouple and found to stay below 30°C for the duration of the process. The resultant solution in chamber A was then pipetted out of the reaction vessel for further processing and analysis, and the unreacted solution in chamber B was discarded. MNPs synthesized via APM in water (under the same plasma parameters with no MBAm) were also prepared as a reference for comparison.

### 2.3 | Formation of thermal-responsive hydrogel

The resultant MNP/MBAm solution was reacted with PNIPAm to form a crosslinked network. Specifically, 500 mg PNIPAm was dissolved in 5 mL of the previously prepared MNP/MBAm solution (NIPAm/MBAm mass ratio of 20:1), followed by addition of 25  $\mu$ L APS solution (10 wt %) and 10  $\mu$ L TEMED. The resulting solution was then placed in the fridge at 4°C overnight to allow the reaction to complete.

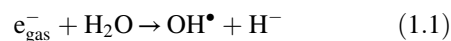
### 2.4 | Characterization

X-Ray Diffraction (XRD, PANalytical X'PERT ProMPD) was used to analyze the crystallinity of the MNPs. Magnetic properties of the MNPs and the magnetic hydrogel were characterized using Vibration Scanning Magnetometry (VSM, Princeton Measurements Corporation Micromag 3900). Fourier Transform Infrared (FTIR, Perkin Elmer Spectrum 100 ATR) spectroscopy was performed to investigate the nature of the chemical bonding in the hydrogel nanocomposite. Samples for the above characterization techniques were prepared by drop-casting the MNP/PNIPAm hydrogel on to Si wafer (for VSM and FTIR analysis) or a glass slide (for XRD analysis) and allowing to dry. The thermal response of the hydrogel composite was tested by heating a 5 mL sample in a thermal bath at 38°C and monitoring until full phase conversion had occurred. The LCST was measured via a thermocouple immersed in the sample solution. Immediately following this, the samples were immersed in a thermal bath at room temperature (approx. 19°C) and the reversible transition back to solution state was monitored. The thermal response of the hydrogel composite was compared to that of a pure PNIPAm hydrogel.

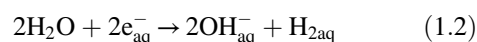
Geometry, size distributions, and further structural analysis of the MNPs were carried out using Transmission Electron Microscopy (TEM, Tecnai G2 F20 S-TWIN, FEI). Particle size distribution and lattice spacing were analyzed by measuring particle dimensions using “FIJI” software package. This involved defining the dimensions of the image relative to the scale bar and then drawing a line across the diameter of each NP and measuring this distance. This was carried out for approx. 50 individual NPs to ensure statistical significance.

## 3 | RESULTS AND DISCUSSION

Our previous work on APM synthesis of NPs has shown that electrons injected into the liquid may either react directly with metal ions in solution or react with water molecules to form short-lived intermediate radicals, which initiate a cascade of further chemical reactions.<sup>[5]</sup> Wang et al.<sup>[10]</sup> expanded on this work to propose a mechanism by which  $\text{Fe}^{2+/3+}$  cations react with hydroxide ions to form  $\text{Fe}_3\text{O}_4$ . Electrons at the interface with the solution are expected to form hydroxyl radicals (1.1).



Once solvated, electrons may also quickly react via second-order recombination to form hydroxide ions and hydrogen (1.2)<sup>[3]</sup>



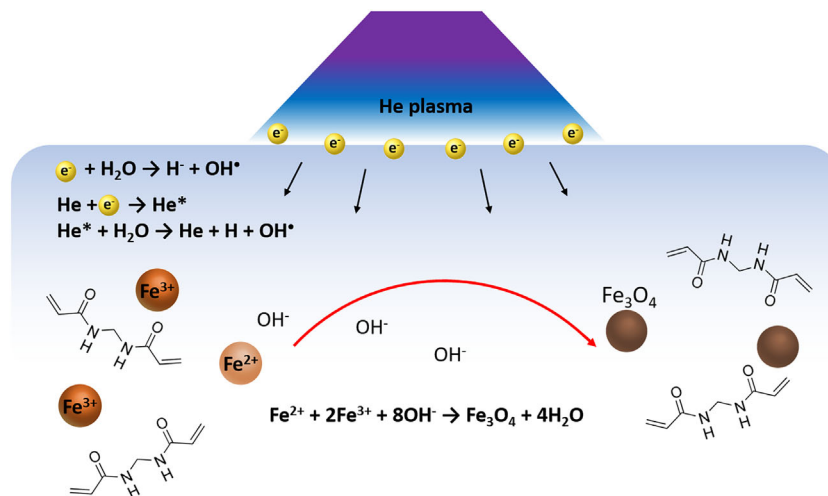
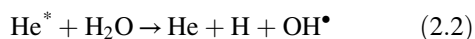
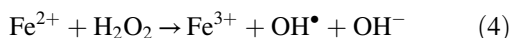
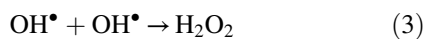


**FIGURE 2** Illustration of the proposed reaction scheme for APM synthesis of MNPs in MBAm solution

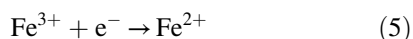
$\text{OH}^\bullet$  may also be formed via interaction of water molecules with metastable helium species at the plasma/liquid interface (2.1, 2.2)



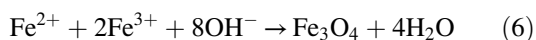
This is believed to cause a cascade of further reactions, producing hydrogen peroxide (3) and hydroxide ions (4).



The ratio of  $\text{Fe}^{2+}:\text{Fe}^{3+}$  is maintained by reaction of excess  $\text{Fe}^{3+}$  with electrons injected from the plasma (5).



Finally, hydroxide ions react with the  $\text{Fe}^{2+/3+}$  cations to form  $\text{Fe}_3\text{O}_4$  (6).



The proposed reaction scheme ensures a steady supply of  $\text{OH}^-$ , facilitating the synthesis of  $\text{Fe}_3\text{O}_4$ . In contrast, coprecipitation techniques rely on the addition of excess  $\text{OH}^-$  to the  $\text{Fe}^{2+/3+}$  solution in a short space of time, which may lead to uncontrolled precipitation of  $\text{Fe}_3\text{O}_4$ . The APM synthesis technique allows for the supply of reactants to be controlled via the plasma parameters (current, gas flow rate, etc). The presence of the stable hydrophilic monomer MBAm in the reaction system could potentially serve as a stabilizer, as the solution containing as-synthesized MNPs remains stable

and shows no signs of precipitation even after long period of time (days).

Degradation of the MBAm in solution during the APM process was minimized due to the small quantity of MBAm (0.5 wt%) present in the reaction solution coupled with mechanical stirring during the plasma processing (which is a low temperature process,  $<30^\circ\text{C}$ ). Although dissociation/fragmentation of MBAm is possible, in our case no significant modifications of the hydrogel chemistry (FTIR) or physical properties (thermal response) have been found after the APM processing (see results sections). The overall reaction scheme in the present work has been summarized in Figure 2.

The resulting mixture after the APM processing was then subjected to a crosslinking process with PNIPAm, after which a MNP/hydrogel composite can be obtained. The crystalline structure of the resulting composite was confirmed by XRD, Figure 3. The broad diffraction peaks present in Figure 3 arise due to the large fluorescent background from the glass substrate. The peaks are in good agreements with those of the Crystallography Open Database pattern 9002026 for  $\text{Fe}_3\text{O}_4$ . This confirms that  $\alpha\text{-Fe}_2\text{O}_3$  has not been formed, as would be expected in an oxygen-rich environment. It should be noted

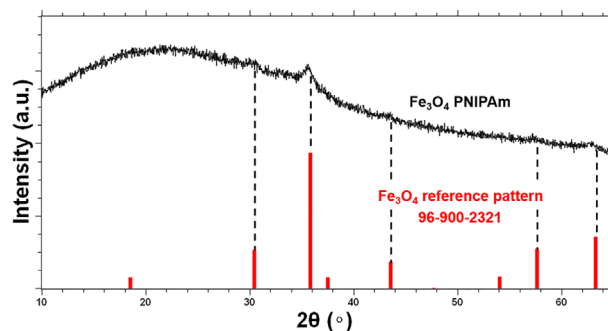


**FIGURE 3** XRD pattern for MNPs synthesized in polymer (black). Reference pattern for  $\text{Fe}_3\text{O}_4$  (COD: 9002026) shown in red

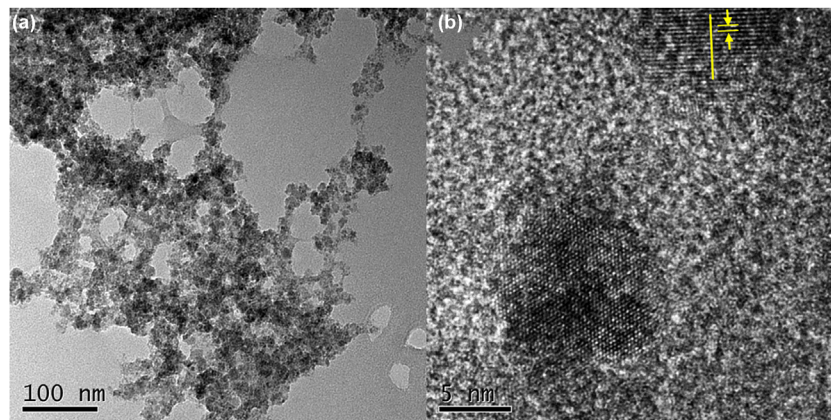


**FIGURE 4** TEM images of (a) Magnetic hydrogel (b) individual particles within the hydrogel with lattice spacing measured

that  $\text{Fe}_3\text{O}_4$  is known to produce a pattern similar to that of  $\gamma\text{-Fe}_2\text{O}_3$  owing to the spinel structure present in both materials. In this study, the 2:1 ratio of  $\text{Fe(III)}:\text{Fe(II)}$  in the salt solution and inert atmosphere should ensure that  $[\text{Fe}^{2+}]:[\text{Fe}^{3+}]$  does not change during the synthesis process. However, in the case of unexpected over-oxidation,  $\gamma\text{-Fe}_2\text{O}_3$  might also form and give the same XRD pattern. This should not adversely affect the magnetic properties of the resultant MNP/PNIPAm composite, as  $\gamma\text{-Fe}_2\text{O}_3$  NPs also exhibit superparamagnetism.<sup>[42]</sup>

TEM analysis revealed information regarding the size, shape and crystal structure of the synthesized MNPs. Figure 4a shows a typical image of the magnetic hydrogel sample, where most MNPs are spherical in shape with a tight particle size distribution (average diameter  $9 \pm 0.97$  nm). Figure 4b shows a typical MNP with lattice fringes clearly visible and the average lattice spacing found to be  $\sim 0.295$  nm, potentially of the (220) plane of  $\text{Fe}_3\text{O}_4$ .<sup>[43]</sup> Analysis of MNPs synthesized via APM in water (the same plasma parameters) with no MBAm found that particles also exhibit consistent lattice spacing, indicating that the presence of MBAm has no role in the MNPs synthesis process and has not modified the crystal structure of the resulting MNPs.

Figure 5 shows the FTIR spectra of the pure PNIPAm, the MNP/PNIPAm composite hydrogel as well as PNIPAm crosslinked with APM treated MBAm (no  $\text{Fe}_3\text{O}_4$  NPs). Typically, PNIPAm exhibits a peak known as Amide I at approx.  $1625\text{--}1650\text{ cm}^{-1}$ , which is associated with stretching vibrational mode of the  $\text{C}=\text{O}$  group in the amide of the PNIPAm chains.<sup>[44,45]</sup> The peak observed at approx.  $1550\text{ cm}^{-1}$  is known as Amide II, and arises due to vibrations of the NH group in the PNIPAm amide. FTIR spectroscopy shows that APM treatment of the MBAm solution has negligible effects on the chemical bonding of the resultant PNIPAm (Figure 5b), compared to PNIPAm prepared without any APM treatment step (Figure 5a). The emergence of a shoulder at  $1640\text{ cm}^{-1}$  (Figure 5c) can be attributed to the presence  $-\text{OH}$  groups on the  $\text{Fe}_3\text{O}_4$  surface.<sup>[46,47]</sup> The result shows that the APM treatment has no direct effect on the chemistry of the PNIPAm.

Magnetization measurements for the crosslinked magnetic hydrogel composite and APM-synthesized MNPs (prepared in water under the same plasma processing parameters, but with no hydrogel components) have been carried out, see Figure 6. The lack of hysteresis for both samples is characteristic of superparamagnetism, a behavior typical in MNPs with

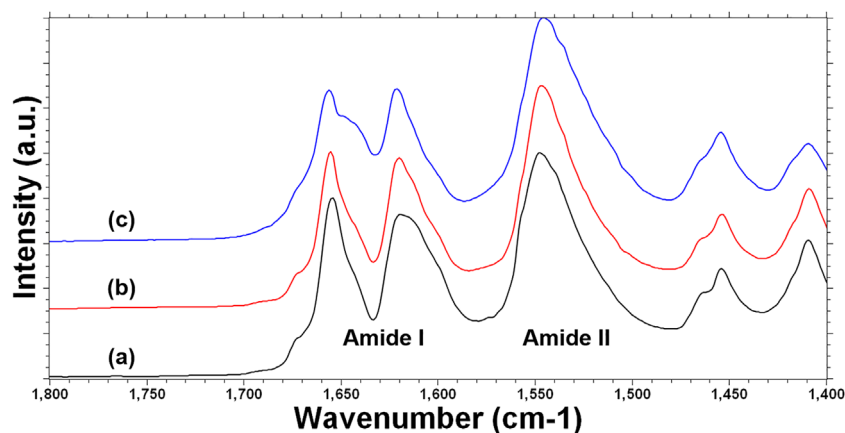


**FIGURE 5** FTIR spectra for (a) pure PNIPAm, (b) PNIPAm crosslinked with AMP-treated MBAm, and (c) the MNP/PNIPAm composite

diameters below approximately 15 nm.<sup>[35]</sup> The observed saturation magnetization ( $M_s$ ) for the magnetic hydrogel sample was approx.  $8.6 \text{ emu g}^{-1}$ , whereas the  $M_s$  for water sample was  $\sim 4.5 \text{ emu g}^{-1}$ . The level of  $M_s$  seen in our study is similar to a previous study in which  $\text{Fe}_3\text{O}_4$  NPs were synthesized using pulsed plasma in liquid containing a cationic surfactant.<sup>[48]</sup> The magnetic properties of MNPs can be affected by many parameters, such as crystallinity, size, shape, and crystal defect density as well as the degree of agglomeration of the material.<sup>[49]</sup> The presence of MBAm during the synthesis process may have influenced the  $M_s$  value of the magnetic hydrogel sample, however, the specific nature of the interaction between MBAm and the MNPs during the APM process requires more detailed investigation in the future.

The thermal response of the MNP/PNIPAm composite hydrogel was compared to that of an equal volume of pure PNIPAm. Both samples were simultaneously immersed in an oil bath held at  $38^\circ\text{C}$  and monitored for phase change. The LCST was observed to be approx.  $33^\circ\text{C}$  for both samples. Complete conversion to the gel state took approx. 5 min in each case, with no evidence of the MNPs significantly changing the phase transition speed. Figure 7a shows images of the phase transition process taking place at 30 s intervals. The translucent sample color corresponds to the liquid solution state at lower temperature below the LCST. Both solutions become milky and stiff when temperature is above the LCST. After 3 min the volume of the sample in contact with the glass vial had fully transitioned to the gel state, while a further 2 min was required for the remainder of the material in the centre of the sample volume to form the gel state. The MNPs were observed to remain stably dispersed in the PNIPAm throughout, with no evidence of them being forced out forming agglomerates during the phase transition. Upon cooling (Figure 7b), both samples returned to the liquid solution state at a rate with no measurable difference. The

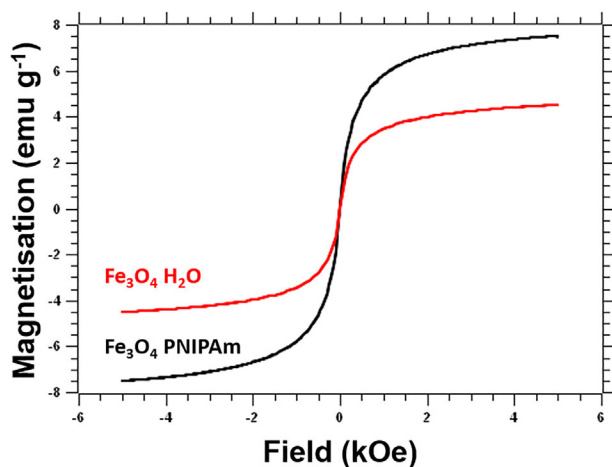


**FIGURE 6** Magnetization curves of the MNPs synthesized in water (red) and the magnetic hydrogel (black)

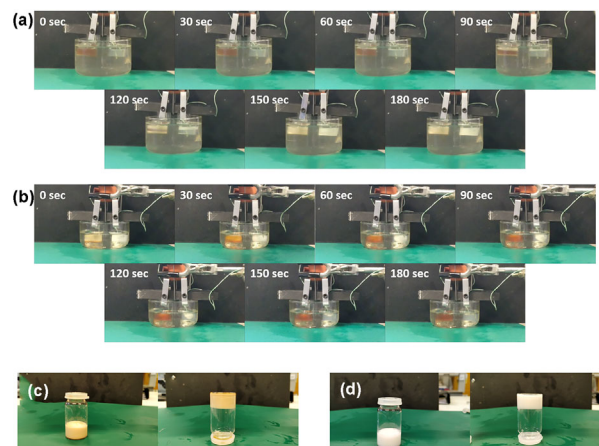


**FIGURE 7** Thermal response of  $\text{Fe}_3\text{O}_4$ /PNIPAm composite hydrogel and pure PNIPAm under (a) heating and (b) cooling across the LCST. (c)  $\text{Fe}_3\text{O}_4$ /PNIPAm composite hydrogel and (d) pure PNIPAm above the LCST, showing gel phase

phase transition could be performed multiple times ( $>10$ ) with no change in behavior noted.

## 4 | CONCLUSIONS

We have successfully demonstrated the synthesis of a magnetic thermo-sensitive hydrogel incorporating APM synthesized magnetic nanoparticles. The chemical composition and physical properties of the resulting hydrogel were not found to be significantly modified by this synthetic route. Indeed, the magnetization of the magnetic hydrogel sample showed a more enhanced magnetic performance compared to MNPs synthesized directly in water. The resultant magnetic hydrogel system was also found to exhibit a reversible phase change at temperatures of interest for biomedical applications. Future work has been planned to characterize magnetic nanocomposites for practical applications such as MRI imaging, drug delivery, and hyperthermia applications. The material produced in this study could be of interest in a range of applications, highlighting the potential of APM technology as a synthetic route for the fabrication of hydrogel nanocomposites in fields such as biomedical, environmental, microfluidics, and sensing.

## ACKNOWLEDGEMENT

The authors would like to acknowledge EPSRC (EP/P00394X/1 and EP/M024938/1) for funding support.

## ORCID

Hugo Nolan <http://orcid.org/0000-0003-3262-6860>

Davide Mariotti <http://orcid.org/0000-0003-1504-4383>

Dan Sun <http://orcid.org/0000-0002-5100-2749>

## REFERENCES

- [1] D. Mariotti, R. M. Sankaran, *J. Phys. Appl. Phys.* **2010**, *43*, 323001.
- [2] D. Mariotti, J. Patel, V. Švrček, P. Maguire, *Plasma Process. Polym.* **2012**, *9*, 1074.
- [3] P. Rumbach, D. M. Bartels, R. M. Sankaran, D. B. Go, *Nat. Commun.* **2015**, *6*, 7248.
- [4] C. Richmonds, R. M. Sankaran, *Appl. Phys. Lett.* **2008**, *93*, 131501.
- [5] J. Patel, L. Němcová, P. Maguire, W. G. Graham, D. Mariotti, *Nanotechnology* **2013**, *24*, 245604.
- [6] T. Yan, X. Zhong, A. Evelyn Rider, Y. Lu, S. A. Furman, Kostya (Ken) Ostrikov, *Chem. Commun.* **2014**, *50*, 3144.
- [7] S. Askari, I. Levchenko, K. Ostrikov, P. Maguire, D. Mariotti, *Appl. Phys. Lett.* **2014**, *104*, 163103.
- [8] Y. Shimizu, A. C. Bose, T. Sasaki, D. Mariotti, K. Kirihara, T. Kodaira, K. Terashima, N. Koshizaki, *Trans. Mater. Res. Soc. Jpn.* **2006**, *31*, 463.
- [9] D. Carolan, C. Rocks, D. Babu Padmanaban, P. Maguire, V. Svrcek, D. Mariotti, *Sustain. Energy Fuels* **2017**, *1*, 1611.
- [10] R. Wang, S. Zuo, W. Zhu, J. Zhang, J. Fang, *Plasma Process. Polym.* **2014**, *11*, 448.
- [11] C. Du, M. Xiao, *Sci. Rep.* **2014**, *4*, 7339.
- [12] T. Velusamy, A. Liguori, M. Macias-Montero, D. B. Padmanaban, D. Carolan, M. Gherardi, V. Colombo, P. Maguire, V. Svrcek, D. Mariotti, *Plasma Process. Polym.* n. d., *14*, 1600224.
- [13] C. Ni, D. Carolan, C. Rocks, J. Hui, Z. Fang, D. B. Padmanaban, J. Ni, D. Xie, P. Maguire, J. T. S. Irvine, D. Mariotti, *Green Chem.* **2018**, *20*, 2101.
- [14] W. Yan, Z. J. Han, B. T. Phung, K. (Ken) Ostrikov, *ACS Appl. Mater. Interfaces* **2012**, *4*, 2637.
- [15] R.-C. Zhang, D. Sun, R. Zhang, W.-F. Lin, M. Macias-Montero, J. Patel, S. Askari, C. McDonald, D. Mariotti, P. Maguire, *Sci. Rep.* **2017**, *7*, 46682.
- [16] H. Nolan, D. Sun, B. G. Falzon, S. Chakrabarti, D. Babu Padmanaba, P. Maguire, D. Mariotti, T. Yu, D. Jones, G. Andrews, D. Sun, *Plasma Process. Polym.* **2018**. <https://doi.org/10.1002/ppap.201800112>.
- [17] Y. Liu, D. Sun, S. Askari, J. Patel, M. Macias-Montero, S. Mitra, R. Zhang, W.-F. Lin, D. Mariotti, P. Maguire, *Sci. Rep.* **2015**, *5*, srep15765.
- [18] S. Mitra, S. Cook, V. Švrček, R. A. Blackley, W. Zhou, J. Kovač, U. Cvelbar, D. Mariotti, *J. Phys. Chem. C* **2013**, *117*, 23198.
- [19] R.-C. Zhang, D. Sun, A. Lu, S. Askari, M. Macias-Montero, P. Joseph, D. Dixon, K. Ostrikov, P. Maguire, D. Mariotti, *ACS Appl. Mater. Interfaces* **2016**, *8*, 13567.
- [20] C. de las Heras Alarcón, S. Pennadam, C. Alexander, *Chem. Soc. Rev.* **2005**, *34*, 276.
- [21] E. Caló, V. V. Khutoryanskiy, *Eur. Polym. J.* **2015**, *65*, 252.
- [22] E. M. Ahmed, *J. Adv. Res.* **2015**, *6*, 105.
- [23] M. I. Baker, S. P. Walsh, Z. Schwartz, B. D. Boyan, *J. Biomed. Mater. Res. B Appl. Biomater.* **2012**, *100B*, 1451.
- [24] N. S. Satarkar, D. Biswal, J. Zach Hilt, *Soft Matter* **2010**, *6*, 2364.
- [25] S. Mornet, S. Vasseur, F. Grasset, P. Veverka, G. Goglio, A. Demourgues, J. Portier, E. Pollert, E. Duguet, *Prog. Solid State Chem.* **2006**, *34*, 237.
- [26] S. Kumaraswamy, S. H. Mallaiiah, *Radiat. Eff. Defects Solids* **2016**, *171*, 869.
- [27] A. C. Manikas, A. Papa, F. Causa, G. Romeo, P. A. Netti, *RSC Adv.* **2015**, *5*, 13507.
- [28] Y. Li, G. Huang, X. Zhang, B. Li, Y. Chen, T. Lu, T. J. Lu, F. Xu, *Adv. Funct. Mater.* **2012**, *23*, 660.
- [29] C. S. S. R. Kumar, F. Mohammad, *Adv. Drug Deliv. Rev.* **2011**, *63*, 789.
- [30] J. Dobson, *Drug Dev. Res.* **2006**, *67*, 55.
- [31] N. S. Satarkar, J. Z. Hilt, *J. Controlled Release* **2008**, *130*, 246.
- [32] R. Hergt, S. Dutz, R. Müller, M. Zeisberger, *J. Phys. Condens. Matter* **2006**, *18*, S2919.
- [33] Y. Jun, J.-H. Lee, J. Cheon, *Angew. Chem. Int. Ed.* **2008**, *47*, 5122.
- [34] Q. A. Pankhurst, J. Connolly, S. K. Jones, J. Dobson, *J. Phys. Appl. Phys.* **2003**, *36*, R167.
- [35] W. Wu, Z. Wu, T. Yu, C. Jiang, W.-S. Kim, *Sci. Technol. Adv. Mater.* **2015**, *16*, 023501.
- [36] H. Liu, C. Wang, Q. Gao, X. Liu, Z. Tong, *Acta Biomater.* **2010**, *6*, 275.
- [37] R. Massart, *IEEE Trans. Magn.* **1981**, *17*, 1247.
- [38] A.-H. Lu, E. L. Salabas, F. Schüth, *Angew. Chem. Int. Ed.* **2007**, *46*, 1222.
- [39] S. G. Starodubtsev, E. V. Saenko, M. E. Dokukin, V. L. Aksenov, V. V. Klechkovskaya, I. S. Zanaevskina, A. R. Khokhlov, *J. Phys. Condens. Matter* **2005**, *17*, 1471.
- [40] R. Messing, N. Frickel, L. Belkoura, R. Strey, H. Rahn, S. Odenbach, A. M. Schmidt, *Macromolecules* **2011**, *44*, 2990.
- [41] N. Shirai, T. Yoshida, S. Uchida, F. Tochikubo, *Jpn. J. Appl. Phys.* **2017**, *56*, 076201.
- [42] Y. Prado, N. Daffé, A. Michel, T. Georgelin, N. Yaacoub, J.-M. Grenèche, F. Choueikani, E. Otero, P. Ohresser, M.-A. Arrio, C. Cartier-dit-Moulin, P. Saintavit, B. Fleury, V. Dupuis, L. Lisnard, J. Fresnais, *Nat. Commun.* **2015**, *6*, 10139.
- [43] H. Iida, K. Takayanagi, T. Nakanishi, T. Osaka, *J. Colloid Interface Sci.* **2007**, *314*, 274.
- [44] Y. Maeda, T. Higuchi, I. Ikeda, *Langmuir* **2000**, *16*, 7503.
- [45] P. M. Reddy, M. Taha, P. Venkatesu, A. Kumar, M.-J. Lee, *J. Chem. Phys.* **2012**, *136*, 234904.
- [46] C. Azmiyawati, L. Suyati, Taslimah, R. D. Anggraeni, *IOP Conf. Ser. Mater. Sci. Eng.* **2017**, *172*, 012009.
- [47] T. Fouquet, G. Mertz, C. Becker, L. Fetzer, F. Ziarelli, D. Ruch, *Plasma Process. Polym.* **2014**, *11*, 931.
- [48] Z. Kelgenbaeva, E. Omurzak, S. Takebe, Z. Abdullaeva, S. Sulaimankulova, C. Iwamoto, T. Mashimo, *Jpn. J. Appl. Phys.* **2013**, *52*, 11NJ02.
- [49] D. Jin, H. Kim, *Bull. Korean Chem. Soc.* **2018**, *39*, 729.

## SUPPORTING INFORMATION

Additional supporting information may be found online in the Supporting Information section at the end of the article.

**How to cite this article:** Nolan H, Sun D, Falzon BG, Maguire P, Mariotti D, Zhang L, Sun D. Thermoresponsive nanocomposites incorporating microplasma synthesized magnetic nanoparticles—Synthesis and potential applications. *Plasma Process Polym.* 2019;16:e1800128. <https://doi.org/10.1002/ppap.201800128>